Available online at www.sciencedirect.com
SCIENCE DIRECT®
Remote Sensing of Environment 103 (2006) 312–323
Remote Sensing of Environment
www.elsevier.com/locate/rse

# Mapping carbon and water vapor fluxes in a chaparral ecosystem using vegetation indices derived from AVIRIS

David A. Fuentes [a,*], John A. Gamon [a], Yufu Cheng [a], Helen C. Claudio [a], Hong-lie Qiu [b], Zhiyan Mao [a], Daniel A. Sims [c], Abdullah F. Rahman [c], Walter Oechel [d], Hongyan Luo [d]

[a] *Department of Biology and Microbiology, California State University LA, Los Angeles, CA 90032, USA*
[b] *Department of Geography and Urban Analysis, California State University LA, Los Angeles, CA 90032, USA*
[c] *Texas Tech University, Department of Range, Wildlife and Fisheries Management, Box 42125, Lubbock, TX 79409, USA*
[d] *Department of Biology, San Diego State University, San Diego, CA 92182, USA*

Received 10 May 2004; received in revised form 14 September 2005; accepted 20 October 2005

**Abstract**

Using simple models derived from spectral reflectance, we mapped the patterns of ecosystem $CO_2$ and water fluxes in a semi-arid site in southern California during a period of extreme disturbance, marked by drought and fire. Employing a combination of low (~2 km) and high (~16 km) altitude images from the hyperspectral Airborne Visible Infrared Imaging Spectrometer (AVIRIS), acquired between April 2002 and September 2003, and ground data collected from an automated tram system, several vegetation indices were calculated for Sky Oaks field station, a FLUXNET and SpecNet site located in northern San Diego County (CA, USA). Based on the relationships observed between the fluxes measured by the eddy covariance tower and the vegetation indices, net $CO_2$ and water vapor flux maps were derived for the region around the flux tower. Despite differences in the scale of the images (from ~2 m to 16 m pixel size) as well as marked differences in environmental conditions (drought in 2002, recovery in early 2003, and fire in mid 2003), net $CO_2$ and water flux modeled from AVIRIS-derived reflectance indices (NDVI, PRI and WBI) effectively tracked changes in tower fluxes across both drought and fire, and readily revealed spatial variation in fluxes within this landscape. After an initial period of net carbon uptake, drought and fire caused the ecosystem to lose carbon to the atmosphere during most of the study period. Our study shows the power of integrating optical and flux data in LUE models to better understand factors driving surface-atmosphere carbon and water vapor flux cycles, one of the main goals of SpecNet.
© 2006 Published by Elsevier Inc.

*Keywords:* Hyperspectral remote sensing; AVIRIS; Carbon flux; Water vapor flux; Disturbance; Light-use efficiency; Vegetation indices; Modeling.

## 1. Introduction

### 1.1. SpecNet and the carbon cycle and disturbance

SpecNet (short for Spectral Network) builds on the existing capabilities of the flux tower network (FLUXNET) by adding spectral measurements to existing flux tower sites at a range of ecosystems around the world. The hope is that integrating optical and flux sampling can facilitate an understanding of factors controlling terrestrial carbon flux and provide information useful for modeling and validating emerging satellite data products (e.g. MODIS).

A primary SpecNet (short for Spectral Network) goal is to understand the factors controlling the exchange of $CO_2$ and water vapor between terrestrial ecosystems and the atmosphere. If we are to properly estimate regional and global carbon fluxes, it is crucial that we first understand the *controls* on ecosystem photosynthesis and respiration. Examples of these controls might be extreme events or conditions, and variation in vegetation cover types, all of which can influence carbon and water vapor fluxes. This way we might be able to predict more accurately how biosphere-atmosphere carbon fluxes might change in the future.

Recent studies that employ both spectral and eddy covariance measurements have provided new insights into the issue of flux controls. For example, a recent study in an eastern deciduous forest revealed mid-season declines in carbon uptake and corresponding optical properties associated with a mid-season

* Corresponding author.
*E-mail address:* dfuente@calstatela.edu (D.A. Fuentes).

0034-4257/$ - see front matter © 2006 Published by Elsevier Inc.
doi:10.1016/j.rse.2005.10.028

drought (Rahman et al., 2004). Recent studies in chaparral ecosystems (Cheng et al., 2006-this issue; Gamon et al., 2006-this issue; Sims et al., 2006-this issue) have illustrated the application of long-term optical monitoring with a mobile "tram system" for exploring relationships between remotely sensed optical signals (spectral reflectance) and carbon and water vapor fluxes. These studies demonstrate the value of continuous ecosystem monitoring because we can detect the effects of stressful periods or extreme events (e.g. drought and fire) on daily productivity and respiratory activity that may not be captured by occasional field sampling, occasional aircraft flights or periodic satellites overpasses. Severe perturbations provide "natural experiments" that disrupt ecosystem components and their underlying processes and can help us understand ecosystem dynamics and underlying controls. By closely matching the scale of the flux tower footprint, the tram system allows us to develop empirical relationships between spectral reflectance and flux measurement, providing a basis for creating regional flux maps with imaging spectrometry. Linking long-term optical and flux monitoring to periodic overpasses with imaging spectrometers provide a means of developing spatially explicit, calibrated flux images. These multi-scale datasets now provide the basis for new approaches to model carbon and water vapor fluxes based on remotely sensed data.

### 1.2. Modeling approaches

There are three approaches that have been employed to identify and quantify carbon sources and sinks at regional and global scales: (1) atmospheric transport modeling, (2) ecosystem carbon exchange modeling (Battle et al., 2000), and (3) remote sensing driven statistical models (Rahman et al., 2001, 2004; Sims et al., 2006-this issue) that are based on the concept of light-use efficiency (Monteith, 1977). The first two of these approaches are highly complex and sophisticated and require a large number of parameters that are often scarce or not available at the spatial and temporal scale necessary (Liu et al., 1999; Randerson et al., 2002). The third approach on the other hand is simple in that it derives its parameters directly from remote sensing and calibrates them with ground eddy covariance measurements. Recent studies employing aircraft (AVIRIS) and satellite (MODIS) data in boreal and deciduous forest ecosystems demonstrate the viability of this third approach (Rahman et al., 2001, 2004).

### 1.3. Light-use efficiency models

The light-use efficiency concept was first introduced by (Monteith, 1977), and it states that net primary productivity (or net carbon gain, typically expressed on an annual basis) is a function of the amount of absorbed photosynthetically active radiation (APAR) and the efficiency (ε) with which vegetation coverts the APAR into biomass.

$$\mathrm{NPP} = \varepsilon * \mathrm{APAR} \quad (1)$$

Recent studies have indicated that both of these parameters can be derived directly from remote sensing, as discussed below.

Numerous studies have shown that the normalized difference vegetation index (NDVI) has a very close relationship with the fraction of PAR absorbed by green vegetation (*f*APAR) (Goward & Huemmrich, 1992; Kumar & Monteith, 1981; Myneni & Williams, 1994; Tucker & Sellers, 1986; Whiting et al., 1992). Thus Eq. (1) can be reformulated as follows:

$$\mathrm{NPP} = \varepsilon * f(\mathrm{NDVI}) * \mathrm{PAR} \quad (2)$$

In the above equation NDVI is converted to the fraction of absorbed photosynthetically active radiation (*f*PAR), which is then multiplied by the incident photosynthetically active radiation (PAR) to derive the absorbed APAR. PAR can be obtained from meteorological stations. To derive the efficiency term, the photochemical reflectance index (PRI) has been used (Table 2). This index was originally derived at the leaf-to-stand scale over diurnal time courses. It has been shown to closely track the daily conversion of xanthophyll cycle pigments (carotenoid pigments associated with the photosynthetic reaction centers and associated with photoprotection under stress) (Gamon et al., 1992, 1997; Peñuelas et al., 1995). Over longer time frames, PRI closely matches the changing carotenoid and chlorophyll levels in synchrony with seasonally changing photosynthetic activity (Sims & Gamon, 2002; Stylinski et al., 2002). Xanthophyll and carotenoid levels change with prevailing conditions and are indicators of photosynthetic down-regulation under stress. Thus, PRI potentially provides a tool for assessing light-use efficiency remotely. Further work has confirmed that PRI can provide a scaleable index of stand-level light-use efficiency (Gamon et al., 2001) and can be applied to larger "pixel sizes" particularly for closed-canopy stands such as those found in heavily vegetated regions (Gamon & Qiu, 1999; Stylinski et al., 2002). Recent work has demonstrated that remotely derived PRI often scales well with whole-stand light-use efficiency and net ecosystem photosynthetic rates, or net ecosystem exchange (NEE), assessed by eddy covariance across a range of ecosystems and stand structures (Nichol et al., 2000; Rahman et al., 2001, 2004). However, other studies have indicated that canopy and stand structure (Barton & North, 2001; Filella et al., 2004) and severe stress (Sims et al., 2006-this issue) can degrade the PRI–flux relationship. Thus, a goal of this study was to explore the effects of severe ecosystem perturbation on the ability of PRI and light-use efficiency models to track ecosystem carbon flux during periods of extreme stress.

In practice, NPP can be derived from Net Ecosystem Exchange (NEE), also called net ecosystem flux, which is commonly measured by eddy covariance over shorter time integrals (half hourly or daily intervals). After incorporating PRI, Eq. (2) can then be reformulated as follows:

$$\mathrm{NEE} = f(\mathrm{PRI}) * f(\mathrm{NDVI}) * \mathrm{PAR} \quad (3)$$

In this study, we explored the application of this model to a chaparral stand with a stand structure that was highly variable due to disturbance. During this study, this stand was exposed to wet and dry years, as well as wildfire, providing a unique opportunity to explore the effects of these extreme conditions on carbon and water vapor fluxes.

### 1.4. Limitations of water on carbon flux

Sims et al. (unpublished results) studied the effects of temperature and water availability in several chaparral species and concluded that water availability was the primary factor limiting light-use efficiency (LUE). At large scales, there are several indices that have been shown to be good indicators of leaf, canopy, and stand water content such as the 970 nm water band index (WBI) (Peñuelas et al., 1993) (Table 2), the normalized difference water index (NDWI) (Gao, 1996) (Table 2), and equivalent water thickness (EWT) (Gao & Goetz, 1995; Roberts et al., 1997). Serrano et al. (2000) showed a strong relationship between leaf water content from ground data and $WBI_{970}$ derived from AVIRIS for chaparral vegetation when canopy cover was greater than 70%. Claudio et al. (2006-this issue) showed that $WBI_{970}$ had a strong link to both water vapor and carbon dioxide fluxes at a chaparral site, suggesting the possibility for deriving flux models with this index.

### 1.5. Goals

The primary goal of this study was to explore whether vegetation indices (NDVI, PRI and water content indices) calculated from AVIRIS and calibrated against ecosystem flux measurements can be used in conjunction with an automated tram acquisition system to derive carbon and water flux maps for semi-arid chaparral ecosystems. Previously, such "physiological mapping" has focused on forest-dominated ecosystems (Rahman et al., 2001, 2004) or on grassland-dominated ecosystems (Gamon et al., 1993). A second goal was to explore the effects of extreme disturbance (both drought and fire) on surface-atmosphere fluxes in a semi-arid chaparral ecosystem. Since arid and semi-arid areas and fire-prone areas comprise large areas of the terrestrial surface, we expect that results from this study will be of wide application for other similar ecosystems around the world. In this study we used two sources of hyperspectral data that have very different spatial scales: AVIRIS (~2–16 m pixels, varying with altitude) and ground data collected using an automated sampling system (~1 m pixels). Thus, a third objective was to compare data from different optical sampling platforms at multiple spatial scales.

## 2. Methods

### 2.1. Site

The area employed in this study is located at Sky Oaks Field station (33° 22′ 25″ N, 116° 37′ 19″ W) (Fig. 1). This site is part of FLUXNET, Ameriflux, and the emerging SpecNet network. Located in the mountains of northern San Diego County (Calif., USA) at an elevation of ~ 1260 m, the higher elevations of this site were dominated primarily by chaparral species, including chamise (*Adenostoma fasciculatum*), manzanita (*Arctostaphylos pungens*), and redshank (*Adenostoma sparsifolium*), and desert

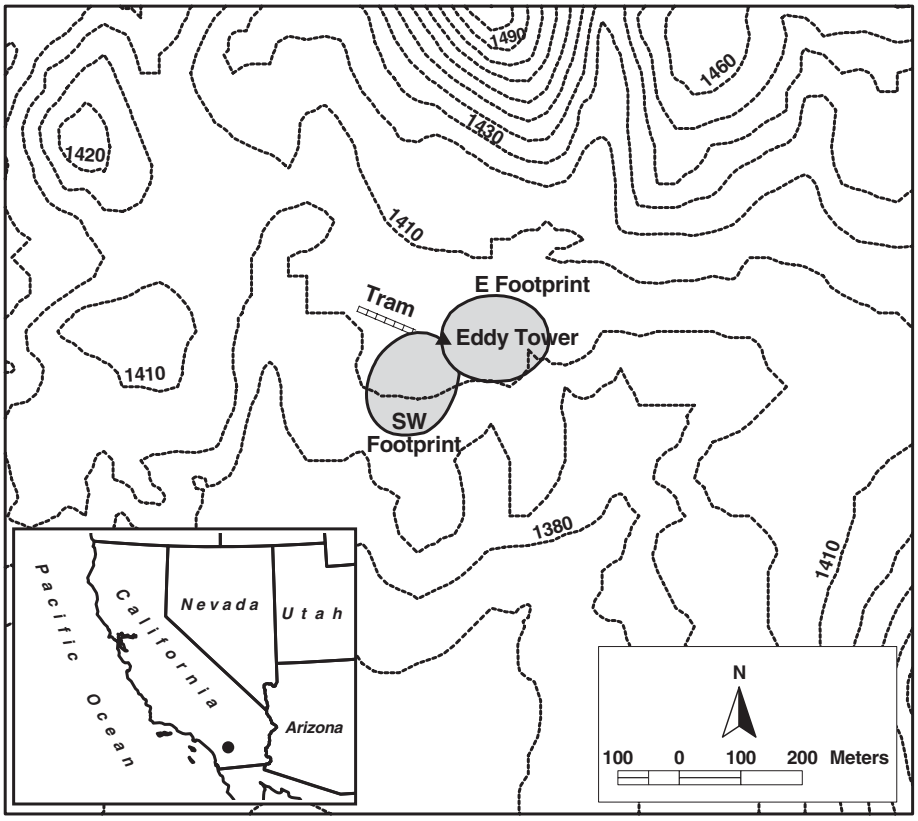


Fig. 1. Illustration of the extent and location of our 1.3 × 1.4 km study area and three sub-areas (the automated cart system or tram, and the E and SW footprints) in relation to the Sky Oaks eddy covariance tower. This area was selected because it had the biggest overlap in all five AVIRIS images. The contour lines shown are spaced at 10 m above sea level intervals. The dot in the inset shows the location of Sky Oaks field station in California, USA.

Table 1
List of dates for AVIRIS flights and their corresponding author pixel ground resolution

| Flight date | Pixel size (m) | Vegetation state |
|---|---|---|
| April 13, 2002 | 2.8 | Beginning of drought |
| July 18, 2002 | 15.8 | Drought |
| October 3, 2002 | 2.3 | Drought |
| March 12, 2003 | 2.7 | Recovery from drought |
| September 10, 2003 | 15.7 | Post-fire recovery |

The state of the ecosystem at the time of the flight is also shown.

ceanothus (*Ceanothus greggii*). Additional cover types in this region included coast live oak (*Quercus agrifolia*), primarily in the washes and riparian corridors. Eddy covariance measurements have been taken at this site since the spring of 1997 (Sims et al., 2006-this issue).

In addition to the eddy covariance tower, this site has a *tram system* that was set up in Summer 2000 to automate the process of collecting spectral data adjacent to the primary tower sampling regions (Fig. 1). The tram consists of a portable hyperspectral spectrometer (UniSpecDC, PP Systems, Haverhill, MA, USA), and an infrared thermometer (model# IRTS-P, Apogee Instruments, Logan, UT, USA) mounted on an automated cart that rides on a 100 m track, crossing representative cover types. Over the study period, cover estimates for the region sampled by the tram ranged from nearly 100% prior to disturbance, to 0% following fire.

The tram system was designed to provide repeated, non-intrusive sampling of ecosystem thermal and optical properties, and thus, it can allow the comparison of vegetation indices at a spatial scale comparable to that of eddy flux measurements. An additional advantage is that it can be operated repeatedly over both diurnal and seasonal scales, and therefore it can allow the study of temporal changes in structural and physiological components of optical signals in ways not possible with single-pass remote sensing (e.g. single AVIRIS overflights). In this study, we took advantage of repeated AVIRIS flights, spanning wet and dry periods, and pre- and post-fire, providing a challenging test of the light-use efficiency model.

Our analysis covers the period of time between April 2002 and July 2003 for which we have matching hyperspectral remotely sensed data from AVIRIS and the tram as well as flux data from the eddy covariance tower. This period provided the unique opportunity to explore the effects of drought and fire, two severe disturbances that recur in this area as well as many other regions of the world: During 2002, southern California experienced the driest year in record and on July 16th, 2003, the Sky Oaks field station burned during the Coyote Fire. All of the eddy covariance equipment and the automated tram system were destroyed, providing a temporary gap in the data. Since then both systems have been rebuilt, and both optical and flux measurements have resumed.

### 2.2. Eddy covariance data and footprints

Net ecosystem $CO_2$ exchange (NEE), or net $CO_2$ flux, water vapor flux, and PAR data were collected for a period of 2 weeks around each AVIRIS flight (Table 1). To explore different temporal aggregation schemes, these data were then divided into three different sets: mean daily values for the week prior to each flight, for the week after, and for the same day of the flight, all of which yielded similar seasonal patterns. The carbon dioxide and water vapor fluxes for these three data sets are shown in Fig. 2A and B, respectively. By examining midday wind direction data for the eddy tower, Sims et al. (2006-this issue) found two dominant wind directions. About 2/3 of the time, the wind came from the southwest and about 1/3 from the east. With this information, we calculated two dominant flux tower "footprints" (sampling regions) using a Flux Source Area Model (FSAM-2.0) (Schmid, 1994). Note that the tram line was positioned on the north edge of the primary (southwest) footprint (Fig. 1), and one goal was to examine the homogeneity of these footprints in terms of their ecosystem fluxes. These sampling areas in relation to the flux tower are shown in Fig. 1. In this study, we compared modeled fluxes from these different footprint regions as a test of landscape homogeneity in the flux values.

### 2.3. AVIRIS and tram vegetation indices

The Airborne Visible Infrared Spectrometer (AVIRIS) acquires hyperspectral data between 400 and 2400 nm, with an approximate bandwidth of 10 nm (Green et al., 1998). The

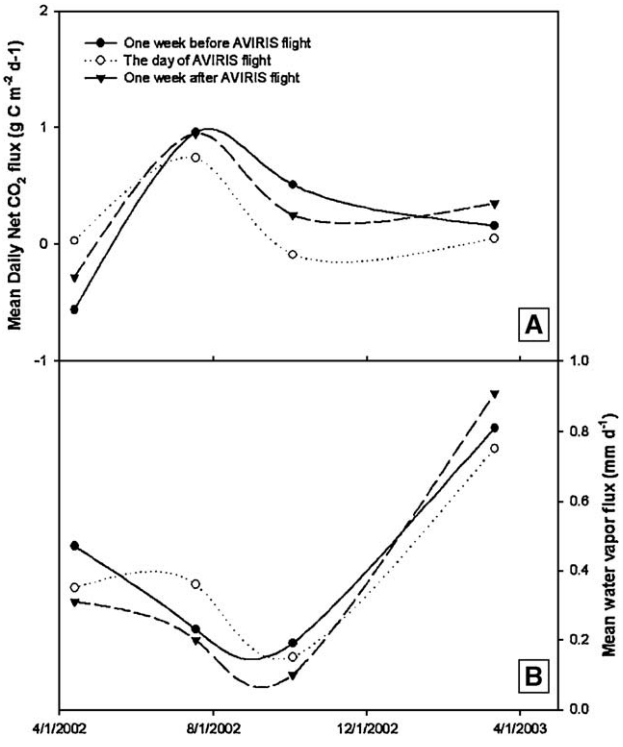


Fig. 2. Seasonal pattern of daily mean net $CO_2$ (A) and water vapor (B) fluxes as measured by the eddy covariance tower at Sky Oaks field station. The data for 2 weeks around each AVIRIS flight was split into three time periods to test temporal effects on the relationship between the vegetation indices and fluxes. For $CO_2$ fluxes, negative values indicate carbon uptake by the ecosystem while positive values carbon release. For water fluxes, higher values indicate larger flux rates between the vegetation and the atmosphere.

ground pixel size of the images can vary between ~2 m and ~16 m depending on the altitude of the flight. For this study, a total of five images were used. These were acquired between April 2002 and September 2003, and spanned wet and dry periods, as well as pre- and post-fire periods. Table 1 shows the flight dates and pixel size of each flight as well as the state of the ecosystem for each acquisition. For all AVIRIS images, the largest common area possible, 1.3×1.4 km, was cut out from the original AVIRIS flight lines to facilitate the analysis (Fig. 1). The radiance images were converted to apparent surface reflectance using radiative transfer software (ACORN, ImSpec LLC, WA, USA). Once converted to reflectance, the vegetation and water indices were calculated two ways: 1) indices were calculated for each pixel, and then averaged for all pixels within a given footprint, and 2) the average reflectance for each footprint was determined, and then indices were calculated from these average reflectance values for each footprint. Because indices are dependent upon spatial scale (grain size), these two methods yielded slightly different values. The first method provided a large sample of "small pixel" indices for each footprint, allowing us to apply statistical methods to compare footprints and sampling platforms, while the second method provided a single "large pixel" index value for each footprint, more suitable for scaling and modeling average ecosystem properties. Consequently, for statistical analysis, we used the first, "small pixel" method, and for modeling and subsequent graphical presentation, we used the second, "large pixel" method.

Table 2 shows the indices and their formulation. The reflectance at the precise wavelengths entered in the equations was determined by interpolation using a linear interpolation routine found in the remote sensing software package ENVI (Research Systems, Inc, CO, USA).

To derive the APAR from AVIRIS, we first converted NDVI values to *f*PAR using the equation:

$$f\mathrm{PAR} = 1.24 * \mathrm{NDVI} - 0.168 \quad (4)$$

This equation uses a strong ($R^2$=0.95) linear relationship between NDVI and *f*PAR and was derived using NDVI and *f*PAR field data across a wide range of southwestern US ecosystems including samples from Sky Oaks field station (Sims et al., 2006-this issue). Then we calculated APAR using the relationship:

$$\mathrm{APAR} = f\mathrm{PAR} * \mathrm{PAR}_{\max} \quad (5)$$

In the above equation, $\mathrm{PAR}_{\max}$ is the daily maximum PAR for the day of AVIRIS flights, obtained from the eddy covariance tower. We did not use the midday PAR values, which were closer to the time of AVIRIS flights, because there was a large gap in the flux tower PAR data for July 18, 2002, which would have reduced our data to only three points. Then, we converted PRI values into an efficiency term by applying the procedure outlined by Rahman et al. (2001, 2004). Theoretical PRI values can range between −1 and +1. To make them all positive with a range from 0 to 1, we used a simple algebraic manipulation of adding 1 to each PRI value and dividing the result by 2. The resulting term was labeled "scaled PRI" (sPRI). Lastly, we derived Net ecosystem $CO_2$ exchange (NEE) using different variations of our simple light-use efficiency model and extracted the mean values for both footprints and the area along the tram from the AVIRIS images:

$$\mathrm{NEE} = f(\mathrm{sPRI}) * \mathrm{APAR}(\mathrm{model\ 1}) \quad (6)$$

$$\mathrm{NEE} = f(\mathrm{sPRI}) * f\mathrm{PAR}(\mathrm{model\ 2}) \quad (7)$$

$$\mathrm{NEE} = f(\mathrm{sPRI}) * f(\mathrm{NDVI})(\mathrm{model\ 3}) \quad (8)$$

For water vapor flux analysis, we derived WBI using two different formulations (Table 2). We used the traditional WBI developed for canopy and leaf data centered around 970 nm in combination with the reference wavelength at 900 nm (Peñuelas et al., 1993). Recent studies (Sims & Gamon, 2003) suggested that the spectral regions 1150–1260 nm and 1520–1540 nm might detect water content better than shorter wavelength indices when using satellite remote sensing data. Thus, we chose the water band centered around 1530 nm, to calculate a second water index. To test the 1150–1260 region, we selected the normalized difference water index (NDWI) developed by Gao (1996) using the AVIRIS imagery. This index uses the reflectance at 860 nm as a reference wavelength and the 1240 nm liquid water absorption band. Lastly we also included the equivalent water thickness (EWT), or canopy water content, image output from the atmospheric correction program ACORN (ImSpec LLC, WA, USA). The formulation for all of these water indices is given in Table 2.

Table 2
Vegetation indices used in our correlation and regression analysis

| Index | Formulation | Function | Reference |
|---|---|---|---|
| PRI | $(R_{531}-R_{570})/(R_{531}+R_{570})$ | Xanthophyll cycle pigment activity | Gamon and Surfus (1999) |
| NDVI | $(R_{800}-R_{680})/(R_{800}+R_{680})$ | Green vegetation cover | Modified from Tucker (1979) |
| $WBI_{970}$ | $R_{900}/R_{970}$ | Leaf, canopy water content | Peñuelas et al. (1997) |
| $WBI_{1530}$ | $R_{900}/R_{1530}$ | Leaf, canopy water content | Sims and Gamon (2003) |
| NDWI | $(R_{860}-R_{1240})/(R_{860}+R_{1240})$ | Leaf, canopy water content | Gao (1996) |
| EWT | From atmospheric correction | Surface liquid water content | ImSpec LLC (2002) |

### 2.4. Correlation and regression analysis

The values needed for our net $CO_2$ flux and water vapor flux models—sPRI, NDVI, $WBI_{970}$, $WBI_{1530}$, NDWI, and equivalent water thickness (EWT)—were extracted from the AVIRIS imagery for both tower footprints and the area along the tram (100×20 m and 100×6 m for high and low altitude flights, respectively). Subsequently, we correlated the modeled fluxes derived from each of these indices to the eddy covariance measurements for net carbon and water vapor fluxes for the

three time periods previously selected (one week prior to, one week after and for the day of each AVIRIS flight). The best correlations observed between the measured net $CO_2$ exchange and remote sensing-based flux models were then applied to the imagery to derive our AVIRIS carbon flux maps. Similar empirical methods were conducted for water vapor flux and various optical indices of water status to derive water vapor flux maps. In order to test the strength and significance of the relationships observed, we used the adjusted $R^2$ and Fisher's "*p* value" (see Results, below).

## 3. Results

### 3.1. Temporal trends of indices and disturbance

Fig. 3 compares AVIRIS-derived index values for each of the three footprints (two tower footprints and tram footprint) to the field-derived data from the tram system. AVIRIS-derived index values for the three footprints showed very similar temporal patterns and absolute magnitudes, suggesting similar vegetation cover for these three areas. Tram PRI showed similar temporal trends as AVIRIS-derived PRI, but showed a "damped" response (higher values were lower, and lower values were higher than AVIRIS-derived PRI values, Fig. 3B). Tram-derived WBI had a higher magnitude WBI for the corresponding AVIRIS-derived footprint, but again showed similar seasonal patterns (Fig. 3C). For most dates, comparisons of the tram to the AVIRIS data indicated that the NDVI values for the tram and AVIRIS data were statistically indistinguishable (student's *t*-tests, based on "small pixel" NDVI values, not shown). However, on most dates, the PRI and WBI values from the tram and AVIRIS were significantly different (student's *t*-test, based on "small pixel" PRI and WBI values, not shown).

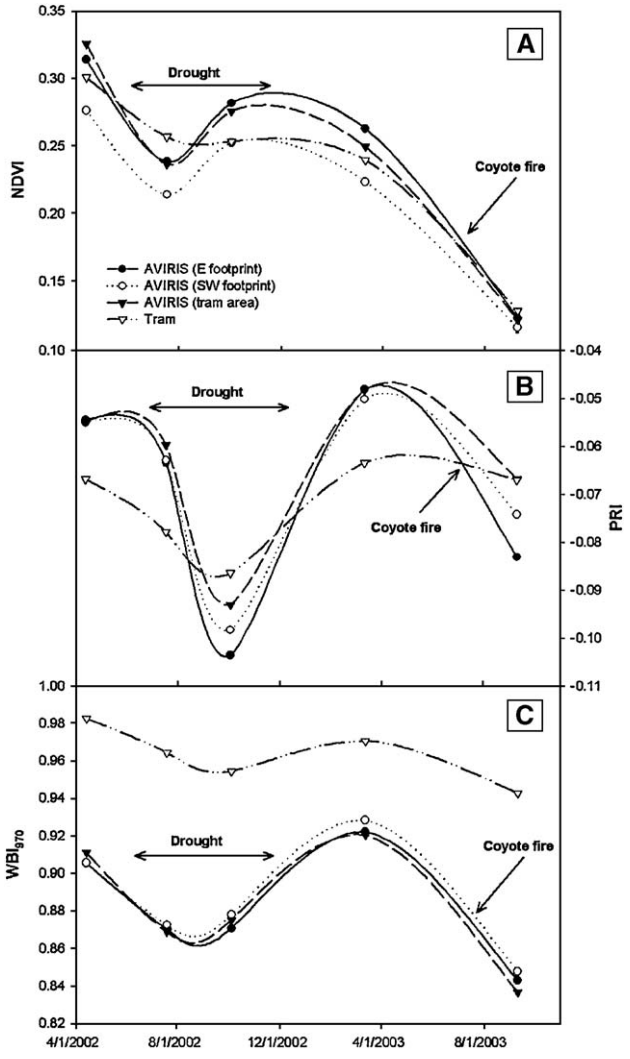


Fig. 3. Seasonal pattern for the normalized difference vegetation index (NDVI) (A), the photochemical reflectance index (PRI) (B), and the 970 nm water band index ($WBI_{970}$)(C). The index values shown were calculated using mean reflectance data for the AVIRIS imagery for our three sub-study areas, and for the ground measurements using the tram system.

The cycle of drought-recovery-fire is also captured well by both AVIRIS and tram datasets for all three indices. All of the indices show a very noticeable decrease during the summer and early fall and a gradual rise at the end of 2002 and the beginning of 2003 (Fig. 3), although the phases of these responses varied slightly between indices. In particular, PRI appears to lag behind NDVI and WBI, showing a delayed dip with drought and a delayed recovery following drought. Post-drought recovery in index values in the winter of 2002–2003 is then followed by a large decline (particularly in NDVI and WBI) associated with the July 16th, 2003 wildfire that burned the entire area.

### 3.2. Carbon flux and indices

The correlations between daily carbon flux from the eddy tower and the different indices calculated for our study areas are shown in Table 3a–c. One of the most striking results from our analysis is that NDVI alone had a high correlation with all expressions of carbon flux studied, while PRI was only weakly correlated. Combining PRI with NDVI improved the correlation with carbon flux slightly over NDVI alone, as has previously been reported for other sites (e.g. Rahman et al., 2001, 2004). Another surprising result was that multiplying the efficiency term sPRI by *f*PAR (model 2) worked much better that the model that incorporated weather station PAR data (i.e., the APAR data, model 3). A slightly higher correlation was seen between the modeled and measured flux values for the week after the AVIRIS flights and the E footprint. Consequently, using model 2, we developed a linear regression model between net measured $CO_2$ flux (NEE) values and the modeled fluxes based on this relationship.

The resulting equation had the following structure:

$$\mathrm{NEE} = a - b^{*}(\mathrm{sPRI}^{*}f\mathrm{PAR}) \text{or} \tag{9}$$

$$\mathrm{NEE} = 2.461 - 26.701(\mathrm{sPRI}^{*}f\mathrm{PAR}) \tag{10}$$

The regression results are shown in Fig. 4. The regression includes values for only four data points because the post-fire flight image had no matching flux data (missing final point) since the eddy covariance tower had burned. The model had an adjusted $R^2 = 0.96$ and $p$ value $= 0.014$.

Table 3
Pearson's correlation coefficients for the daily net $CO_2$ flux for our three study areas (E footprint, SW footprint, and tram areas), and PRI, NDVI, sPRI×APAR (model 1), sPRI×*f*PAR (model 2), and sPRI×NDVI (model 3)

| | sPRI | NDVI | sPRI×NDVI | sPRI×fPAR | sPRI×APAR |
|---|---|---|---|---|---|
| E footprint (A) | | | | | |
| Daily net $CO_2$ flux (1 week prior to AVIRIS flight) | −0.389 | −0.891 | −0.967 * | −0.937 | −0.791 |
| Daily net $CO_2$ flux (day of AVIRIS flight) | 0.275 | −0.738 | −0.660 | −0.700 | −0.286 |
| Daily net $CO_2$ flux (1 week after AVIRIS flight) | −0.059 | −0.981 * | −0.978 * | −0.986 * | −0.786 |
| SW footprint (B) | | | | | |
| Daily net $CO_2$ flux (1 week prior to AVIRIS flight) | −0.391 | −0.791 | −0.884 | −0.837 | −0.723 |
| Daily net $CO_2$ flux (day of AVIRIS flight) | 0.281 | −0.662 | −0.610 | −0.639 | −0.280 |
| Daily net $CO_2$ flux (1 week after AVIRIS flight) | −0.060 | −0.920 | −0.947 | −0.936 | −0.757 |
| Tram area (C) | | | | | |
| Daily net $CO_2$ flux (1 week prior to AVIRIS flight) | −0.346 | −0.864 | −0.911 | −0.889 | −0.761 |
| Daily net $CO_2$ flux (day of AVIRIS flight) | 0.308 | −0.583 | −0.533 | −0.558 | −0.261 |
| Daily net $CO_2$ flux (1 week after AVIRIS flight) | −0.012 | −0.931 | −0.928 | −0.931 | −0.764 |

* Correlation is significant at the 0.05 level (2 tailed).

This equation was then applied to all of the AVIRIS images to derive $CO_2$ flux maps. The units of the maps are given in grams of Carbon per square meter per day (g C $m^{-2}$ $d^{-1}$). The resulting images are presented in Fig. 5A–E. For these images negative values indicate carbon sequestration by the ecosystem while positive values carbon release into the biosphere. The highest carbon uptake is observed in the riparian corridors dominated by *Quercus agrifolia*, which shows up more clearly as white areas in the July 2002 image (Fig. 5B). Lower NEE values were exhibited by the tram and flux tower footprints, which were dominated by chaparral species.

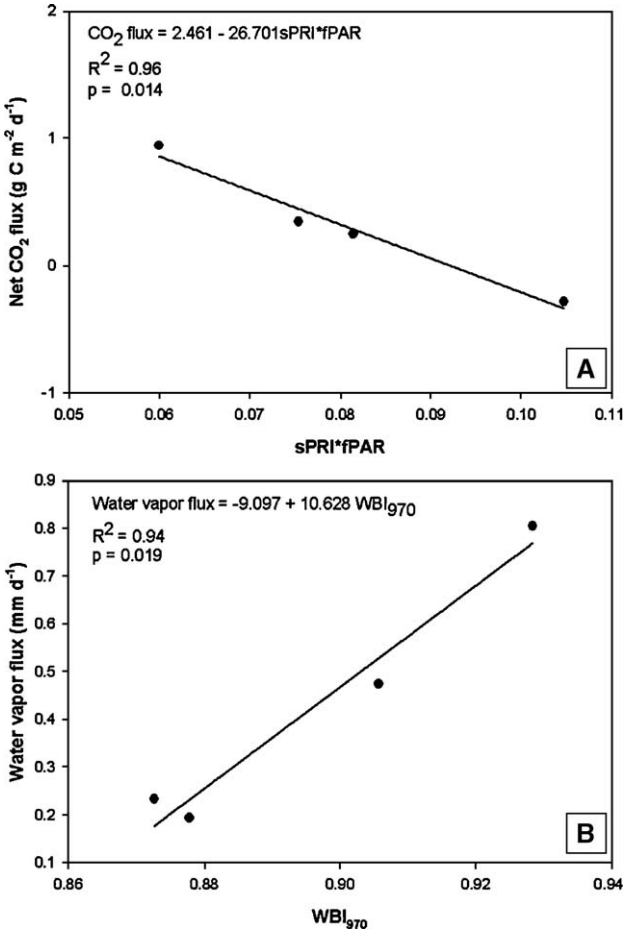


Fig. 4. Linear regression models used to calibrate and map carbon and water fluxes. The net $CO_2$ flux model (A) was developed using the relationship between $CO_2$ flux for the week after AVIRIS flights with the mean sPRI×*f*PAR values from the E footprint area. The water vapor model (B) was derived using flux measurements for the week before AVIRIS flights and the mean $WBI_{970}$ values for the SW footprint.

While the ecosystem began as a carbon sink, it was clearly a source of carbon to the atmosphere following drought (Fig. 6A). Some regrowth during the recovery from drought led to a partial relaxation of the post-drought carbon release, but the ecosystem continued to exhibit a net loss of carbon to the atmosphere. The ecosystem became an even stronger carbon source following fire (Fig. 6A), which removed virtually all leaf area and reduced the green canopy cover to essentially zero (not shown).

The estimated carbon flux derived from the East footprint calibration (Eq. (10)) were applied to all three footprints (two tower footprints and the tram footprint) and then compared to those measured by the flux tower for the week after the AVIRIS flights (Fig. 6A). Regardless of the footprint used, and regardless of the AVIRIS flight altitude, modeled net $CO_2$ fluxes closely followed the measured fluxes through the cycles of drought and partial recovery. Because of the loss of the flux tower in the fire, no post-fire tower flux data were available for comparison at the time of the post-fire AVIRIS flight, but spot soil flux measurements with a gas exchange system (LI-6200, LI-COR Inc, Lincoln, NE, USA) confirmed that the ecosystem was a continuous source of carbon after the fire (data not shown), which is in agreement with the modeled results shown in Fig. 6.

### 3.3. Water vapor flux and indices

Table 4a–c show the correlation analysis results between $WBI_{970}$, $WBI_{1530}$, NDWI and EWT, and the measured water vapor fluxes for our three study periods. Of all the indices tested, $WBI_{970}$ had the highest correlation with all water vapor flux periods while $WBI_{1530}$ and NDWI had the lowest correlations. EWT performed better than $WBI_{1530}$ and NDWI,

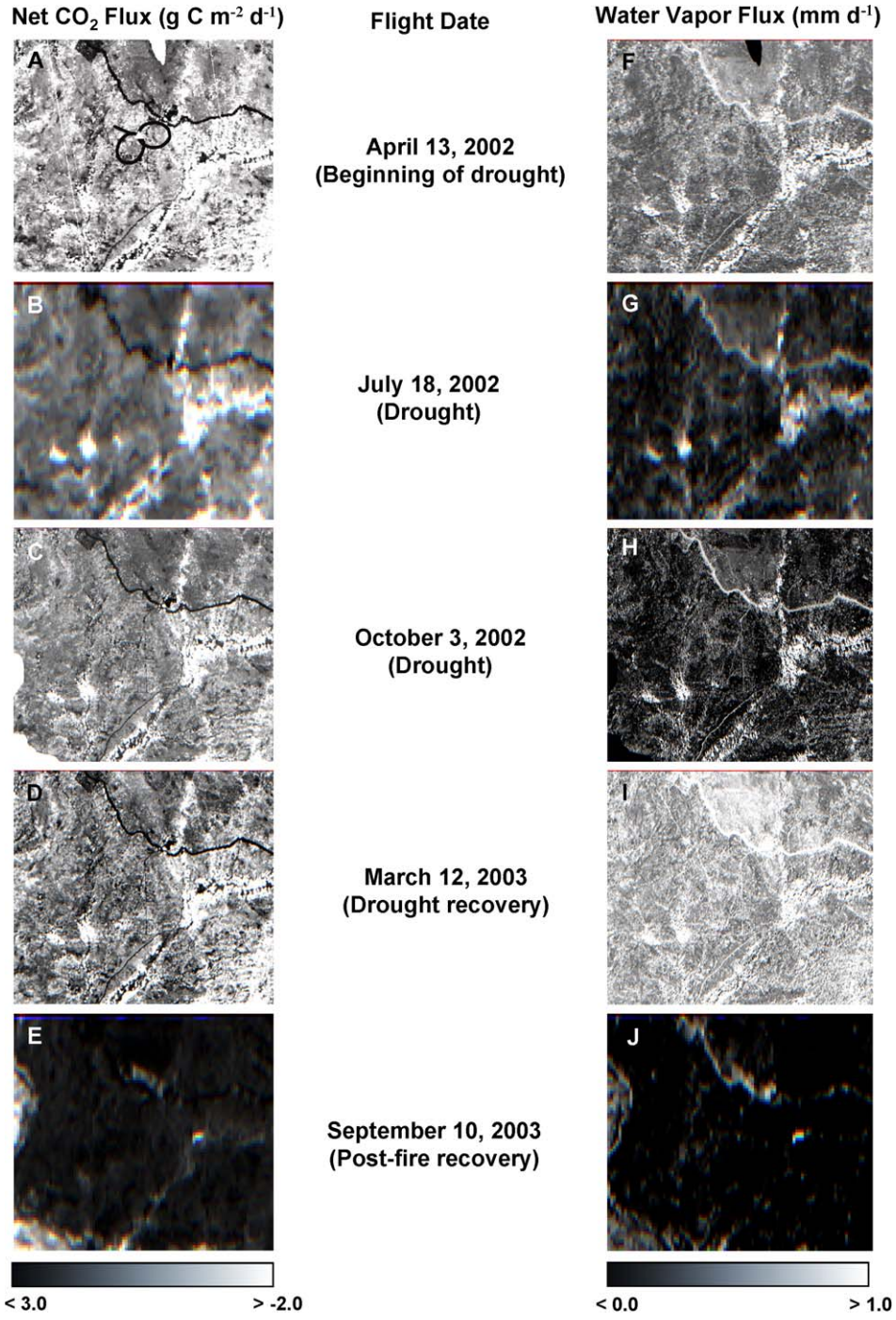


Fig. 5. Net carbon dioxide (A–E) and water vapor (F–J) flux maps derived from AVIRIS. Our three study areas (E and SW footprints and tram area) are shown in A. Higher flux rates (white) are observed for the riparian corridors dominated by *Quercus agrifolia*. (For interpretation of the references to colour in this figure legend, the reader is referred to the web version of this article.).

but the relationships were not statistically significant. Water vapor fluxes for the week before AVIRIS flights correlated better with $WBI_{970}$, and spatially they correlated best with the dominant SW footprint. Following a similar approach used to derive the carbon vapor fluxes, we chose the slightly better correlation between $WBI_{970}$ for the SW footprint and the water vapor flux for the week before AVIRIS flights to develop the linear regression model to map water vapor flux. Again, because of the missing flux data for the July post-fire flight, we could only use four data points in our analysis. The results of the regression model are given in Fig. 4B. It yielded the following equation:

$$\text{Daily water vapor flux} = -9.097 + 10.628\ WBI_{970} \quad (11)$$

With an adjusted $R^2 = 0.94$ and a $p$ value $= 0.019$. Subsequently, we applied our regression model to our five AVIRIS images to produce our water vapor flux maps. The results are presented in Fig. 5F–J, with the units in millimeters of water

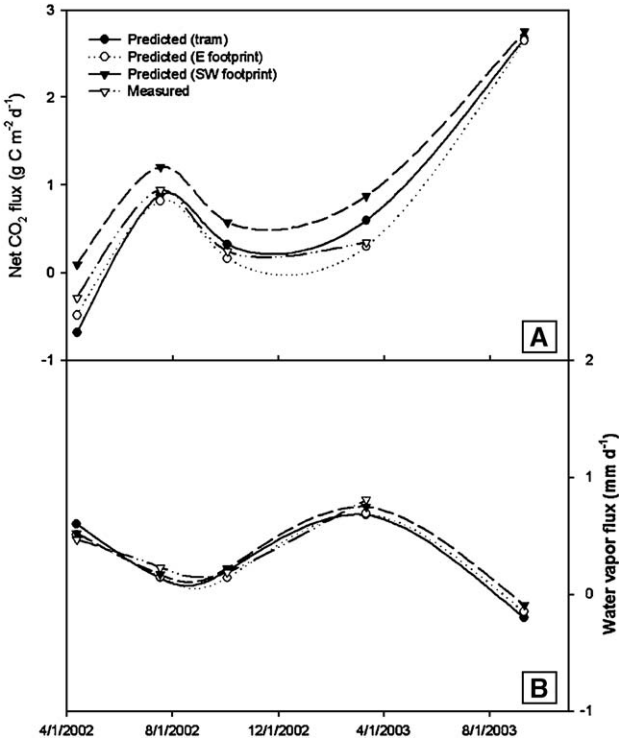


Fig. 6. Comparison of the seasonal patterns of measured $CO_2$ (A) and water vapor (B) fluxes and those predicted from the AVIRIS images using our linear equation models for our three study areas (tram, E and SW footprints. The predicted values for $CO_2$ were calculated using the model developed from the data for the week before the AVIRIS flight for the E footprint. Those for the water vapor were derived using the model that used the data for the week after the flight for the SW footprint. Because the flux tower was destroyed in the July 2003 fire, the last point was estimated using the model only.

vapor per day (mm $d^{-1}$). Following the same analysis to test the soundness of our water flux maps, we extracted the mean predicted values for both of the footprints and the area along the tram from our AVIRIS-derived maps and compared them to the measured water vapor fluxes for the week before our hyperspectral aircraft data. The resulting curves (Fig. 6B) reveal an extremely close match between measured and modeled fluxes, regardless of the footprint used in the model and regardless of the altitude of the AVIRIS flight. Both measured and modeled fluxes revealed a decline in evapotranspiration with drought (summer 2002), followed by recovery to pre-drought levels (winter 2003), and a subsequent decline following the July 16th, 2003, burn.

## 4. Discussion

As expected, the results of our analysis show a strong link between fluxes and optical properties of chaparral vegetation for several of the optical indices studied. In particular, the vegetation indices NDVI, PRI and WBI captured the effects of changing environmental conditions (drought-recovery-fire) on the carbon and water balance. Furthermore, those relationships appeared strong despite the varying pixel size of the AVIRIS imagery.

The differences in the magnitude of index values (particularly PRI and WBI, Fig. 3) between tram and AVIRIS data could be caused by different landscape regions, different instrument responses, or different atmospheric correction approaches between the field spectrometer (UniSpecDC, PP Systems, Amesbury, MA, USA) and the aircraft spectrometer (AVIRIS), rather than due to sampling scale. Since NDVI and modeled fluxes matched well, we conclude that instrument responses (e.g. bandwidth and radiometric calibration issues) or atmospheric correction issues are the most likely sources of error. Slight instrument differences would tend to show up in PRI and WBI because these indices are based on narrow-band formulations in sloped regions of the reflectance spectrum. NDVI, which is derived from two relatively "flat" spectral bands in the red and NIR would be less sensitive to instrument differences, as seen in Fig. 3. Additionally, incomplete atmospheric correction for aerosol scattering (which preferentially affects short wavebands) or water vapor absorption (which affects water absorption bands) would tend to cause errors in the wavebands used for PRI and WBI far more than they would affect the NDVI wavebands. These effects reveal a serious weakness of these indices that needs to be considered in any attempts to model fluxes at multiple scales, from multiple instruments, or in any effort to validate satellite data with ground data. The empirical calibrations used here (Fig. 4) effectively solve this problem, much as empirical line calibrations can improve atmospheric corrections (ImSpec LLC, 2002). Thus, for accurate cross-scale flux analyses based on remotely sensed data, it appears that some degree of empirical calibration remains necessary. By combining flux and optical sampling at similar scales across multiple ecosystems, the SpecNet network provides an ideal system for sensor intercomparison and calibration.

Table 4
Pearson's correlation coefficients for the mean daily water vapor flux for our three study areas (E footprint, SW footprint, and tram areas), and our four water indices

| | $WBI_{970}$ | $WBI_{1530}$ | NDWI | EWT |
|---|---|---|---|---|
| *E footprint (A)* | | | | |
| Water vapor flux (1 week prior to AVIRIS flight) | 0.970 * | −0.057 | 0.359 | −0.596 |
| Water vapor flux (day of AVIRIS flight) | 0.826 | −0.277 | 0.431 | −0.569 |
| Water vapor flux (1 week after AVIRIS flight) | 0.879 | −0.298 | 0.256 | −0.713 |
| *SW footprint (B)* | | | | |
| Water vapor flux (1 week prior to AVIRIS flight) | 0.981 * | 0.038 | 0.510 | −0.625 |
| Water vapor flux (day of AVIRIS flight) | 0.837 | −0.200 | 0.593 | −0.583 |
| Water vapor flux (1 week after AVIRIS flight) | 0.910 | −0.208 | 0.429 | −0.731 |
| *Tram area (C)* | | | | |
| Water vapor flux (1 week prior to AVIRIS flight) | 0.926 | −0.248 | 0.292 | −0.424 |
| Water vapor flux (day of AVIRIS flight) | 0.732 | −0.548 | 0.285 | −0.484 |
| Water vapor flux (1 week after AVIRIS flight) | 0.803 | −0.479 | 0.139 | −0.596 |

* Correlation is significant at the 0.05 level (2 tailed).

Despite differences in absolute magnitude across instruments, the same seasonal patterns were observed for ground and airborne data, and indicated striking variability in surface-atmosphere fluxes for this ecosystem. This indicates that, with proper calibration, the light-use efficiency model is, in principle, "scaleable" across the range of grain sizes (1 m to 16 m) (Table 1) used in this study, and supports the direct comparison of tram (1 m pixels) to AVIRIS (2–16 m pixels). However, the different absolute values obtained by different instruments (AVIRIS vs. tram-based spectrometer) indicate that careful consideration must be given to sensor effects when comparing or integrating different instruments.

The similar modeled fluxes obtained with all three footprints (the two flux tower footprints and the tram footprint) indicate that the chaparral landscape around the eddy covariance tower is sufficiently homogenous to be treated as a single, coherent stand (i.e., the tram and flux tower footprints all sample similar, representative areas of this ecosystem). This ability to relate optical to flux sampling footprints is an essential prerequisite to validating flux models driven from remote sensing. Additionally, the effects of the severe drought, recovery, and fire were clearly visible in the three primary vegetation indices (NDVI, PRI and $WBI_{970}$), as well as in the modeled fluxes, demonstrating the utility of this method for tracking changes in ecosystem carbon and water vapor fluxes with disturbance.

Our carbon modeling and mapping results differed from previous studies at this and other sites (Rahman et al., 2001, 2004; Stylinski et al., 2002) in certain respects. For example, Rahman et al. (2001) found that for a boreal ecosystem in central Canada, PRI had a strong relationship to gross $CO_2$ flux while that with NDVI was very weak. Similar results had previously been found in this same chaparral ecosystem under more "normal" rainfall years (Stylinski et al., 2002). In contrast, our analysis of this chaparral stand under more extreme events (drought and fire) showed a strong correlation between net $CO_2$ flux and NDVI, while PRI had a relatively weak link to net $CO_2$ flux at the whole-stand scale. Our findings, along with other analyses of the PRI and NDVI responses (Sims et al., 2006-this issue), suggest that the extreme stress (severe drought and fire) experienced in 2002–2003 causes these indices to behave differently than in more favorable, mesic conditions (Rahman et al., 2001; Stylinski et al., 2002). Under more favorable conditions, this chaparral ecosystem resembles an evergreen system, with little changes in canopy structure and more stable NDVI values (Stylinski et al., 2002). Under these conditions, changes in photosynthetic activity were detectable with changes in PRI (e.g. Stylinski et al., 2002). However, the extreme drought of 2002, and the subsequent fire in 2003 caused this normally evergreen system to respond more like a deciduous system, with large changes in canopy structure and associated leaf senescence caused by drought and fire. Under these extreme conditions, "greenness" indices such as NDVI more successfully explained most of the variability in carbon flux. On the other hand, PRI, which is readily confounded by leaf senescence (Gamon et al., 2001) and changes in canopy structure (Barton & North, 2001), becomes less effective as an indicator of carbon flux in such extreme conditions. Similar findings have been reported for a Mediterranean shrubland, where the utility of PRI as a photosynthetic index varied with dynamic factors such as leaf area index, deciduousness, and flowering patterns (Filella et al., 2004). Thus, it appears that the degree of fidelity between PRI and fluxes, even within a single ecosystem, is strongly affected by stand structural traits, including "evergreenness" and the degree of canopy closure, which varied enormously in this ecosystem across time. This dynamic behavior of optical indices due to changing canopy structure within a single ecosystem further suggests that optically based light-use efficiency models require periodic (e.g. seasonal) calibration against flux data, particularly for ecosystems undergoing extreme perturbations in stand structure or physiology. Alternatively, ecosystem flux models that include more explicit consideration of stand structure might improve the fidelity of physiologically based indices such as PRI with whole-ecosystem fluxes. Thus, a remaining challenge will be to develop robust models driven from remote sensing that can clearly isolate the physiological and structural contributions affecting both the fluxes and the optical signals. One simple approach might be the development of modified indices that incorporate the effects stand structure (e.g. the sun-angle-corrected NDVI, Sims et al., 2006-this issue).

The variations in model formulations (Eqs. (6)–(8)) deserve further study. Good results were obtained with the simplest model based on NDVI (Eq. (8)). When we calculated *f*PAR using NDVI (Eq. (7)) the relationship improved a little; however, when we multiplied maximum daily PAR values by *f*PAR to obtain APAR, and used this term in the model (Eq. (6)), the correlation decreased slightly, from −0.986 to −0.786 and became statistically insignificant (Table 3). We originally expected that inclusion of this APAR term would yield the best result, as it considers the actual PAR absorbed and potentially available for photosynthesis. However, due to missing flux tower data during the time of AVIRIS overflight, the actual PAR was estimated from values taken at other times, which presumably introduced error into the model. This result illustrates the potential danger of mixing data sources (e.g. micrometeorological data and remote sensing data), particularly in cases of missing data where interpolation is needed, and the potential strength of models based on single, consistent data sources (i.e. based on remote sensing alone). Clearly, reliable PAR measurements are critical to accurate light-use efficiency models.

The net $CO_2$ flux maps that were produced seem to closely follow net ecosystem $CO_2$ exchange (NEE) as measured by eddy covariance techniques for the areas that we tested. Particularly noticeable is the dramatic changes in net carbon flux for this ecosystem from a sink to a source over a relatively short time period due to drought (between April and July 2002, Fig. 5A–B). Fire further enhanced the carbon loss from this ecosystem. Also, it is evident from the flux maps that there are large differences in responses of the various cover types, e.g. chaparral vs. riparian corridors (white areas in the July image), which are not easily detectable in flux tower data that cannot easily resolve spatial patterns of flux. This striking variability

in surface-atmosphere fluxes due to disturbance and contrasting cover types deserves further attention if we are to fully understand the biotic controls on the terrestrial carbon cycle. This ability of multi-temporal remote sensing to accurately depict both spatial and temporal patterns in ecosystem metabolism during extreme perturbations illustrates the value of adding remote sensing to the flux tower network (FLUXNET), and is a main goal of SpecNet. However, a more exhaustive analysis is needed to examine this modeling approach, with larger datasets and in other areas, and to independently validate the modeled fluxes. An additional flux tower has been set up at Sky Oaks field station in an area that was not burned during the July 2003 fire. Ideally, future AVIRIS flights will include this new tower, which, along with similar studies at other SpecNet sites (e.g. Rahman et al., 2004), this will help to further validate this $CO_2$ flux mapping approach.

One of the most significant and novel findings in this work is the development of a methodology to derive water vapor flux from the strong relationship seen between eddy covariance measurements and the 970-nm water band index ($WBI_{970}$). Although the significant relationship between canopy water content and flux and this particular index has been reported before (Claudio et al., 2006-this issue; Serrano et al., 2000), to our knowledge this is the first time that it has been used to map water vapor fluxes. The better performance of $WBI_{970}$ is somewhat surprising since we also tested indices that were thought to better capture ecosystem water content as seen from aircraft or/and satellite imagery ($WBI_{1530}$ and NDWI; Gao, 1996; Sims & Gamon, 2003), and therefore expected to be better predictors of ecosystem water flux. On the other hand, our finding is consistent with that of Serrano et al. (2000) who found $WBI_{970}$ to be the best index of canopy-level water status from the AVIRIS data. Just as in the case of the carbon flux maps, the predicted water vapor fluxes followed well those measured by the eddy covariance method, regardless of the sampling footprint used in the model (Fig. 6B). The extreme disruption observed for carbon flux during July 2002 as well at the recovery process in fall 2002 and spring 2003 is also seen for water flux. A comparison of carbon and water flux maps shows similar responses to varying disturbance regimes across the study period (Figs. 5 and 6), further illustrating the underlying strong relationship between water and carbon flux (i.e., photosynthesis and respiration are strongly limited by water availability).

It remains unclear whether it is possible to develop a single empirical model parameterization that could be applied across all ecosystems. It is then essential to have cross-site validation and individual model calibration of the optical-flux relationship for a variety of ecosystems and for particular sensors. The basic premise is that while a light-use efficiency (LUE) model is universal, the particular parameterization of the terms of this model (APAR and LUE) may have to consider the vastly differing controls across ecosystems and biomes. Furthermore, explicit treatment of component fluxes (photosynthesis and respiration) must be considered and validated across sites. This kind of cross-site analysis of optical data validated with actual ecosystem flux data has simply not been done, and is a main goal SpecNet.

## 5. Conclusions

Carbon dioxide and water vapor fluxes from tram and AVIRIS data clearly demonstrate the ability of calibrated remote-sensing based light-use efficiency models to accurately track seasonally changing $CO_2$ flux for a semi-arid chaparral ecosystem at the Sky Oaks site. Previous applications of this model had focused on heavily forested areas, such as the boreal forests of central Canada and the eastern deciduous forests of Indiana. We have now successfully tested the applicability of this model to an ecosystem far more structurally complex and prone to extreme drought and fire. Similarly, a simple empirical model derived from the 970 nm water band index (WBI) closely followed the measured water vapor fluxes. The close agreement between measured and modeled fluxes across a severe drought and fire supports the use of these simple optically-based modeling approaches for tracking changing spatial and temporal patterns of carbon dioxide and water vapor fluxes. Our results demonstrate a striking spatial and temporal variability in carbon and water vapor fluxes for this chaparral site. Furthermore, these results highlight the power of integrating optical and flux data sources at matching temporal and spatial scales for model development and validation. In particular, there is a strong need for continuous ground and periodical aircraft optical sampling in order to calibrate and validate satellite products (e.g. MODIS, Cheng et al., 2006-this issue). Models that integrate optical and flux data could also be used to estimate missing flux data ("gap filling"), a common need at flux tower sites due to periods of missing data (Falge et al., 2001). We propose that the addition of hyperspectral aircraft or tram sensors can be used to develop calibrated $CO_2$ and water vapor flux maps from satellite data for flux tower sites. Combined with tower flux measurements, these maps could then provide a spatially explicit understanding of the controls on ecosystem fluxes by different landscape cover types, and could also be used to improve satellite estimates of regional carbon and water vapor fluxes.

## Acknowledgements

This research was funded by a NSF CREST grant. Our thanks goes to JPL's Rob Green and the entire AVIRIS team, Cal. State L.A.'s Center for Spatial Analysis and Remote Sensing for their assistance in the atmospheric correction of the AVIRIS imagery, and the CEA–CREST funded students who helped in the collection of the ground data.

## References

Barton, C. V. M., & North, P. R. J. (2001). Remote sensing of canopy light use efficiency using the photochemical reflectance index — Model and sensitivity analysis. *Remote Sensing of Environment*, *78*, 264–273.

Battle, M., Bender, M. L., Tans, P. P., White, J. W. C., Ellis, J. T., Conway, T., et al. (2000). Global carbon sinks and their variability inferred from atmospheric $O_2$ and $^{13}C$. *Science*, *287*, 2467–2470.

Cheng, Y., Gamon, J. A., Fuentes, D. A., Mao, S., A., S. D., Qiu, H. -L., et al. (2006). A multi-scale analysis of dynamic optical signals in a Southern California chaparral ecosystem: a comparison of field, AVIRIS and MODIS data.*Remote Sensing of Environment*, *103*, 369–378 (this issue). doi:10.1016/j.rse.2005.06.013

Claudio, H. C., Cheng, Y., Fuentes, D. A., Gamon, J. A., Luo, H., Oechel, W., et al. (2006). Monitoring drought effects on vegetation water content and fluxes in a chaparral ecosystem using the 970 nm water band index. *Remote Sensing of Environment*, *103*, 304–311 (this issue). doi:10.1016/j.rse.2005.07.015

Falge, E., Baldocchi, D., Olson, R., Anthoni, P., Aubinet, M., Bernhofer, C., et al. (2001). Gap filling strategies for defensible sums of net ecosystem exchange. *Agricultural and Forest Meteorology*, *107*, 43–69.

Filella, I., Peñuelas, J., Llorens, L., & Estiarte, M. (2004). Reflectance assessment of seasonal and annual changes in biomass and $CO_2$ uptake of a Mediterranean shrubland submitted to experimental warming and drought. *Remote Sensing of Environment*, *90*, 308–318.

Gamon, J. A., Field, C. B., Fredeen, A. L., & Thayer, S. (2001). Assessing photosynthetic downregulation in sunflower stands with an optically-based mode. *Photosynthesis Research*, *67*, 113–125.

Gamon, J. A., Field, C. B., Roberts, D. A., Ustin, S. L., & Valentini, R. (1993). Functional patterns in an annual grassland during an AVIRIS overflight. *Remote Sensing of Environment*, *44*, 1–15.

Gamon, J. A., Peñuelas, J., & Field, C. B. (1992). A narrow-waveband spectral index that tracks diurnal changes in photosynthetic efficiency. *Remote Sensing of Environment*, *41*, 35–44.

Gamon, J. A., & Qiu, H. -L. (1999). Ecological applications of remote sensing at multiple scales. In F. I. Pugnaire, & F. Valladares (Eds.), *Handbook of functional plant ecology* (pp. 805–846). New York: Marcel Dekker, Inc.

Gamon, J. A., Serrano, L., & Surfus, J. S. (1997). The photochemical reflectance index: an optical indicator of photosynthetic radiation use efficiency across species, functional types, and nutrient levels. *Oecologia*, *112*, 492–501.

Gamon, J. A., Sims, D. A., Cheng, Y., Fuentes, D. A., Houston, S., MacKinney, L., et al. (2006). A mobile tram system for systematic sampling of ecosystem optical properties. *Remote Sensing of Environment*, *103*, 246–254 (this issue). doi:10.1016/j.rse.2006.04.006

Gamon, J. A., & Surfus, J. S. (1999). Assessing leaf pigment content and activity with a reflectometer. *New Phytologist*, *143*, 105–117.

Gao, B. C. (1996). NDWI— A normalized difference water index for remote sensing of vegetation liquid water from space. *Remote Sensing of Environment*, *58*, 257–266.

Gao, B. C., & Goetz, A. F. H. (1995). Retrieval of equivalent water thickness and information related to biochemical-components of vegetation canopies from AVIRIS data. *Remote Sensing of Environment*, *52*, 155–162.

Goward, S. N., & Huemmrich, K. F. (1992). Vegetation canopy PAR absorbance and the normalized difference vegetation index: An assessment using the SAIL model. *Remote Sensing of Environment*, *39*, 119–140.

Green, R. O., Eastwood, M. L., Sarture, C. M., Chrien, T. G., Aronsson, M., Chippendale, B. J., et al. (1998). Imaging spectroscopy and the Airborne Visible Infrared Imaging Spectrometer (AVIRIS). *Remote Sensing of Environment*, *65*, 227–248.

ImSpec LLC (2002). *ACORN 4.0 User's Guide.* Boulder, Colorado: ImSpec LCC.

Kumar, M., & Monteith, J. L. (1981). Remote sensing of crop growth. In H. Smith (Ed.), *Plants and the Daylight Spectrum.* San Diego, CA: Academic.

Liu, J., Chen, J. M., Cihlar, J., & Chen, W. (1999). Net primary productivity distribution in the BOREAS region from a process model using satellite and surface data. *Journal of Geophysical Research*, *104*, 27235–27754.

Monteith, J. L. (1977). Climate and the efficiency of crop production in Britain. *Philosophical Transactions of the Royal Society of London. Series B*, *281*, 277–294.

Myneni, R. B., & Williams, D. L. (1994). On the relationship between FAPAR and NDVI. *Remote Sensing of Environment*, *49*, 200–211.

Nichol, C. J., Huemmrich, K. F., Black, T. A., Jarvis, P. G., Walthall, C. L., Grace, J., et al. (2000). Remote sensing of photosynthetic-light-use efficiency of boreal forest. *Agricultural and Forest Meteorology*, *101*, 131–142.

Peñuelas, J., Filella, I., Biel, C., Serrano, L., & Save, R. (1993). The reflectance at the 950–970 nm region as an indicator of plant water status. *International Journal of Remote Sensing*, *14*, 1887–1905.

Peñuelas, J., Filella, I., & Gamon, J. A. (1995). Assessment of photosynthetic radiation-use efficiency with spectral reflectance. *New Phytologist*, *131*, 291–296.

Peñuelas, J., Pinol, J., Ogaya, R., & Filella, I. (1997). Estimation of plant water concentration by the reflectance Water Index (WI) ($R_{900}/R_{970}$). *International Journal of Remote Sensing*, *18*, 2869–2875.

Rahman, A. F., Cordova, V. D., Gamon, J. A., Schmid, H. P., & A., S. D. (2004). Potential of MODIS ocean bands for estimating $CO_2$ flux from terrestrial vegetation: A novel approach. *Remote Geophysical Research Letters*, *31*, L10503. doi:10.1029/2004GL019778.

Rahman, A. F., Gamon, J. A., Fuentes, D. A., Roberts, D. A., & Prentiss, D. (2001). Modeling spatially distributed ecosystem flux of boreal forest using hyperspectral indices from AVIRIS imagery. *Journal of Geophysical Research-Atmospheres*, *106*, 33579–33591.

Randerson, J. T., Enting, I., Schuur, E. A. G., Caldiera, K., & Fung, I. Y. (2002). Seasonal and latitudinal variability of troposphere $D_{14}CO_2$: Post bomb contributions from fossil fuels, oceans, the stratosphere, and the terrestrial biosphere. *Global Biogeochemical Cycles*, *16*, 1112. doi:10.1029/2002GB001876.

Roberts, D. A., Green, R. O., & Adams, J. B. (1997). Temporal and spatial patterns in vegetation and atmospheric properties from AVIRIS. *Remote Sensing of Environment*, *62*, 223–240.

Schmid, H. P. (1994). Source areas for scalar and scalar fluxes. *Boundary-Layer Meteorology*, *67*, 293–318.

Serrano, L., Ustin, S. L., Roberts, D. A., Gamon, J. A., & Peñuelas, J. (2000). Deriving water content of chaparral vegetation from AVIRIS data. *Remote Sensing of Environment*, *74*, 570–581.

Sims, D. A., & Gamon, J. A. (2002). Relationships between leaf pigment content and spectral reflectance across a wide range of species, leaf structures and developmental stages. *Remote Sensing of Environment*, *81*, 337–354.

Sims, D. A., & Gamon, J. A. (2003). Estimation of vegetation water content and photosynthetic tissue area from spectral reflectance: A comparison of indices based on liquid water and chlorophyll absorption features. *Remote Sensing of Environment*, *84*, 526–537.

Sims, D. A., Luo, H., Hastings, S., Oechel, W. C., Rahman, A., & Gamon, J. A. (2006). Parallel adjustments in vegetation greenness and ecosystem $CO_2$ exchange in response to drought in a Southern California chaparral ecosystem. *Remote Sensing of Environment*, *103*, 289–303 (this issue). doi:10.1016/j.rse.2005.01.020

Stylinski, C. D., Gamon, J. A., & Oechel, W. C. (2002). Seasonal patterns of reflectance indices, carotenoid pigments and photosynthesis of evergreen chaparral species. *Oecologia*, *131*, 366–374.

Tucker, C. J. (1979). Red and photographic linear combinations to monitor vegetation. *Remote Sensing of Environment*, *8*, 127–150.

Tucker, C. J., & Sellers, P. J. (1986). Satellite remote sensing of primary production. *International Journal of Remote Sensing*, *7*, 1395–1416.

Whiting, G. J., Bartlett, D. S., Fan, S. M., Bakwin, P. S., & Wofsy, S. C. (1992). Biosphere atmosphere $CO_2$ exchange in tundra ecosystems — Community characteristics and relationships with multispectral surface reflectance. *Journal of Geophysical Research-Atmospheres*, *97*, 16671–16680.